Received July 12, 2020, accepted July 29, 2020, date of publication August 4, 2020, date of current version August 18, 2020.

Digital Object Identifier 10.1109/ACCESS.2020.3014141

Fiber Optic Acoustic Vibration Sensors for Ultrasound Measurement in Low-Pressure CO_2 Environment

JINGCHUAN ZHANG, YIFEI PEI, AND XIYUAN LI
Beijing Institute of Spacecraft Environment Engineering, Beijing 100094, China
Corresponding author: Jingchuan Zhang (jhw101411@hotmail.com)

This work was supported by Beijing Talents Foundation.

ABSTRACT The detection of acoustic signals in the Martian environment is significant to understand the issues such as the evolution of the universe, structure of matter, origin of life, and future migration of humans. We proposed a method for testing ultrasonic wave by using fiber-optic Fabry-Perot vibration sensors in a low-pressure CO_2 environment. We conducted high-precision sound wave amplitude and speed measurement tests with different center frequencies at 21, 25, 34, and 40 kHz under different gas compositions, pressures, and distances. Results showed that under the conditions of 15 °C and gas pressure in the range of 600 Pa to 1 MPa, the measured average sound velocity of ultrasonic signals at each frequency was 268.79 m/s in the CO_2 environment, which was lower than the velocity of 336.18 m/s measured in the air environment. The results in this study can be applied to theoretical and experimental studies of future Mars probes pertaining to ultrasonic positioning and detection.

INDEX TERMS Fiber-optic, Fabry-Perot, ultrasonic, sound velocity, CO_2 gas, low-pressure environment.

I. INTRODUCTION

Mars is one of the most worthy planets to study in the solar system. Characterizing the Martian environment is of great significance to understand the issues such as the evolution of the universe, structure of matter, origin of life, and future migration of humans. Investigations of the atmosphere and climate, space environment, and landforms are important aspects of Mars characterization [1], [2].

The atmosphere of Mars is primarily composed of carbon dioxide (95% carbon dioxide, 2.7% nitrogen, 1.6% argon, 0.13% oxygen, and a small amount of other gases) [3], [4]. As an important means of exploring the surface environment, detecting the distance of objects and positioning remote targets, ultrasonic detection plays a key role in the study of Mars's space environment and landform features. As sound transmission is closely related to factors such as pressure, atmospheric composition, atmospheric density, temperature, humidity, and frequency, the characteristics of sound waves propagating in the atmosphere of Mars must differ from those in the atmosphere of the Earth. The difference in ultrasonic transmission has a great influence on the result of ultrasonic detection. Therefore, it is significant to study the velocity of acoustic signals in the Martian environment.

Starting from various simplified models of atmospheric acoustics, researchers such as Dr. Williams of the University of California [5], Drs. Bass, Chambers of the University of Mississippi [6], Dr. Petculescu of Northwestern University [7], [8], and Dr. Leighton of the University of Southampton, UK [9], [10] used different numerical simulation methods to analyze the characteristics of sound waves in an extremely low pressure environment, as well as the sound velocity and attenuation in carbon dioxide gas. The theoretical analysis results showed that audible sound in the frequency range of 20–20,000 Hz is more severely attenuated on Mars than on Earth. In 1999, the Mars Microphone research team tested an acoustic sensor in a vacuum chamber and confirmed that acoustic signal from 100 Hz to 4000 Hz can be transmitted at a low pressure of 1000 Pa [11]. When the pressure decreased from 10^4 Pa to 10^3 Pa, the acoustic signal gradually weakened as well. However, details of the experiment have not been published, and the gas composition in the vacuum chamber is unknown. Presently, there is little reference information on the propagation characteristics of ultrasonic waves at low pressure, either theoretically or experimentally, especially under low-pressure CO_2 conditions.

The associate editor coordinating the review of this manuscript and approving it for publication was Zhenbao Liu.

To record the acoustic signals on Mars and explore the laws of sound wave propagation in the extreme environment of Mars, studies on the feasibility and propagation characteristics of ultrasonic waves in low-pressure CO_2 environments are urgently needed [12]. This also provides a basis for developing ultrasonic anemometers, exploring applications of ultrasonic sensing technology in detection and early warning systems for vehicles on Mars, and answering key questions such as whether sounds can be transmitted in the atmosphere of Mars [13]. The optical fiber Fabry-Perot (F-P) sensor has high sensitivity and can avoid the effect of electromagnetic interference and low-pressure discharge [14]–[16], which makes it an accurate and effective acoustic vibration monitoring sensor [17]–[20]. In this study, we set up a test system for measuring ultrasonic in a low-pressure gas. Based on the optical fiber F-P vibration sensor, we carried out measurements with center frequencies of 21, 25, 34, and 40 kHz at different distances in environments of different gas composition (air, CO_2) and pressure from 600 Pa to 1 MPa. We also explored the relationship between the amplitude of sound wave and pressure gas composition, frequency and receiving distance. These can provide a reliable theoretical and experimental basis for the subsequent application of research on wind speed measurement, positioning, detection, and recording to the Martian environment.

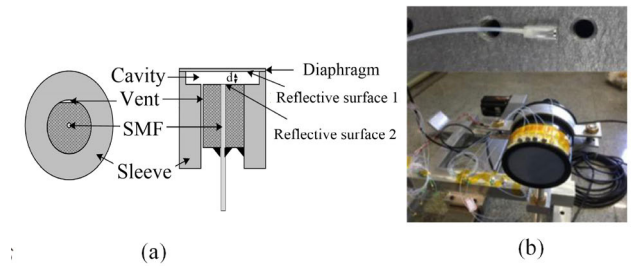

FIGURE 1. (a) Sensor structure diagram and (b) sensor and test system in field.

II. THEORY

The optical fiber F-P vibration sensor used in this study is a diaphragm-extrinsic fiber Fabry-Perot sensor, with the structure shown in Figure 1(a). The ultra-thin film is used as a sensitive element to sense external sound and vibration signals. The micro-cavity of Fabry-Perot sensor is composed of an end face of optical fiber and a sensing diaphragm. The two reflective surfaces of the Fabry-Perot interference structure are composed of an inner diaphragm surface (reflection surface 1) and an optical fiber end face (reflection surface 2). The structure also forms a vertical through-hole between the micro-cavity and the outside atmosphere, such that the micro-cavity can maintain a pressure balance with the outside atmosphere, avoiding the effect of the enclosed gas damping caused by enclosed space in the cavity.

When the external acoustic vibration signal acts on the diaphragm in the form of sound pressure, the diaphragm elastically deforms, causing changes in the length of Fabry-Perot cavity and the intensity of reflected light. The model of Fabry-Perot cavity can be approximated as a two-beam interference pattern, and the intensity of interference output light Ir can be expressed as:

$$I_r = \left(R_1 + R_2 - 2\sqrt{R_1 R_2}\cos\delta\right) I_0 \tag{1}$$

where I_0 is the intensity of incident light; R_1 is the effective reflectivity of reflection surface 1; R_2 is the reflectivity of the fiber end face; and $\delta = 4\pi nL/\lambda_0$, where λ_0 is center wavelength of the light source, n is the refraction index of the medium in the cavity, and d is the cavity length between the two reflective surfaces of the cavity.

The intensity of interference output light I_r is transmitted to the fiber-optic sensor demodulation unit through a single-mode optical fiber. Then, it is processed via photoelectric detection and a signal demodulation circuit to ultimately become a voltage signal. Through phrase demodulation, the change in the length of the cavity d can be obtained, and the original characteristics of the acoustic signal can be restored.

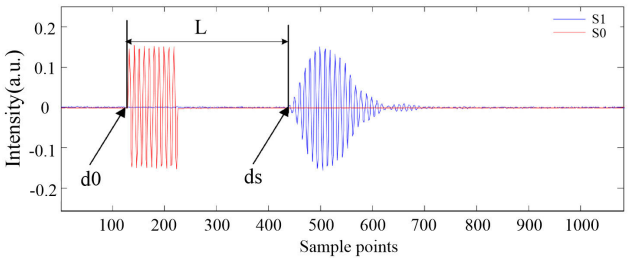

FIGURE 2. Signals of the signal generator and optical fiber F-P vibration sensor.

As shown in Figure 2, the optical fiber sensing demodulation module synchronously collects signals of the signal generator S_0 and optical fiber F-P vibration sensor S_1. There is a certain time difference Δt between the two signals, which can reflect the time needed by the sound wave to travel a certain distance. Therefore, the calculation formula of the sound speed can be expressed as:

$$v = \frac{L}{\Delta t} = \frac{L}{\frac{d_s - d_0}{f_s}} = \frac{L \cdot f_S}{d_s - d_0} \tag{2}$$

where v, L, f_s, d_0, and d_s represent the sound speed, distance between the acoustic transmitting unit and receiving unit, sampling frequency, initial moment of excitation signal by the signal generator, and initial moment when the optical F-P sensor receives the signal.

III. EXPERIMENT

To realize the experimental measurement of the acoustic wave under different conditions of atmospheric pressure and gas composition, we assembled a test system device, which is shown in Figure 3. The test system device is consist of a ring-shaped container, vacuum subsystem, an ultrasonic

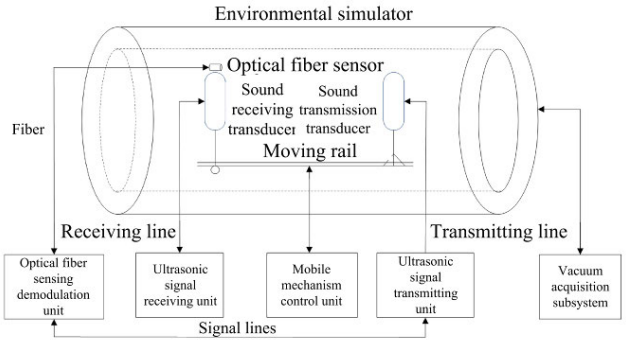

FIGURE 3. Block diagram of test system.

transmitting subsystem, an ultrasonic receiving subsystem, a moving mechanism, and a fiber optic sensing subsystem.

The vacuum subsystem rotary vane pump produces the internal pressure of the environmental simulation container from 600 Pa to 1.0×10^5 Pa, and uses a vacuum gauge to accurately measure the internal pressure of the container. The environmental simulation system is shown in Figure 4.

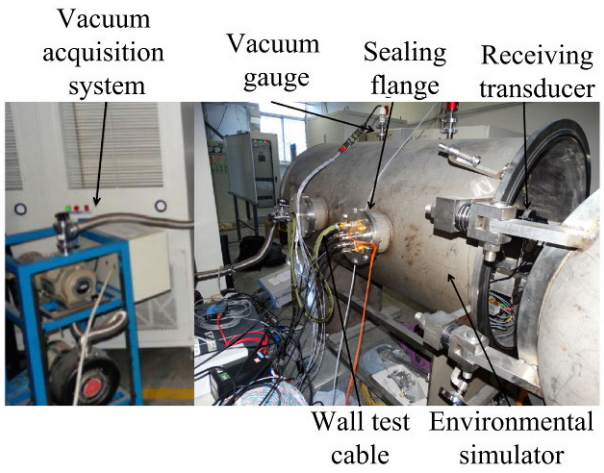

FIGURE 4. The environmental simulation system.

With the environmental simulation container exhibiting an inner diameter of 800 mm, effective length of 1600 mm, and leakage rate of less than 1.0×10^{-4} Pa·L/s, the device can guarantee that under the condition of 600 Pa, the pressure change is less than ± 10 Pa within 5 min, which meets the testing requirement of the pressure holding time. The receiving transducer inside the ring-mode container is connected to the external filtering and amplification circuit of the container through a wall measurement and control cable. The output of the signal filtering and amplification circuit is connected to an oscilloscope to complete the data storage and display mechanism. The interior of the environmental simulation container is shown in Figure 5.

As shown in Figure 6, we assemble a moving mechanism in the environmental simulation container. The slide rail is used to adjust the distance between the sound receiving transducer

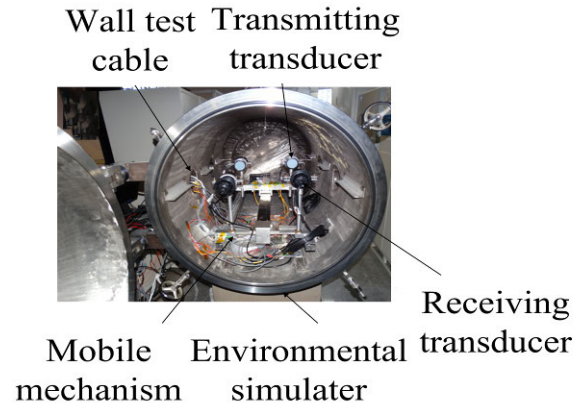

FIGURE 5. Interior of the environmental simulation container.

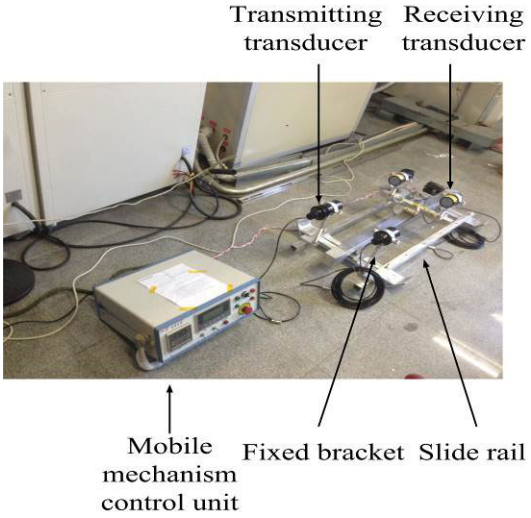

FIGURE 6. The moving mechanism.

and transmitting transducer, as well as reduce the leakage and repression of the ring mold container. This design can ensure that the sound receiving transducer and sound transmitting transducer are in the same testing environment, which avoids the additional effect on ultrasonic propagation caused by the change in the gas composition, the temperature and humidity of the environment.

During the test, we aligned the transmitting transducer with the corresponding receiving transducer. The optical fiber F-P vibration sensors are fixed on the top of the acoustic receiving transducer, aligning the diaphragm of the sensor with the front surface of the receiving transducer. In each experiment, the signal generator generates a signal of certain frequency to drive the acoustic emission unit to emit ultrasonic wave of the corresponding frequency. After propagating a certain distance in the ring mode container, the sound waves reach the sound receiving end.

The optical fiber sensing subsystem is used to detect and demodulate the acoustic signal. As shown in Figure 7, the optical fiber F-P vibration sensors are fixed on top of the

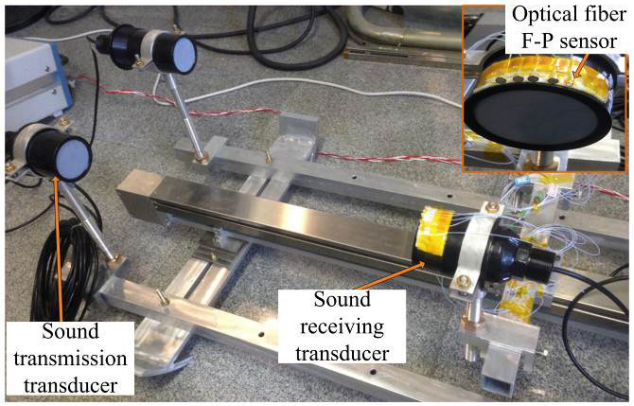

FIGURE 7. Layout of optical fiber sensor.

acoustic receiving transducer, which is also directly in front of the acoustic emission transducer. This makes the diaphragm of the optical fiber F-P vibration sensor rightly face the sound source. After the ultrasonic vibration signal is received by the optical fiber F-P sensor, it is transmitted by the transmission fiber and received by the demodulation module. Then it is read and stored by computer for processing and analysis of the data of subsequent sound velocity.

A. ANALYSIS OF ULTRASONIC ACOUSTIC AMPLITUDE IN ATMOSPHERIC ENVIRONMENT AND CO_2 ENVIRONMENT

To investigate the amplitude of ultrasonic signals at different pressures, we filled the atmosphere inside the ring-shaped container. The 21, 25, 34, and 40 kHz ultrasonic signals are selected for experimental measurements to prove the multi-frequency measurement capabilities of the sensor proposed. Under the test conditions of different pressures and distances, the acoustic signals measured by the optical fiber F-P sensor are shown in Figure 8, where S_0 is the excitation signal of the sound source, and S_1 is the detection signal of the F-P sensor.

It can be seen from results that the optical fiber F-P sensor can adapt to the low-pressure atmospheric environment of 600 Pa while still receiving ultrasonic signals. In order to further investigate the amplitude of ultrasonic signals in different gas environments, the ring-shaped container is filled with CO_2 gas. Under the test conditions of the different pressures and distances, the acoustic signals measured by the optical fiber F-P sensor are shown in Figure 9.

It can be seen from the results that the optical fiber F-P sensor can adapt to the low-pressure 600 Pa CO_2 environment while still receiving ultrasonic signals.

In the optical fiber acoustic vibration sensor, the vibration diaphragm is an elastic flat plate. The edge of the diaphragm is fixed on the metal ring and the support structure, and its deformation and movement are determined by its own material and external mechanical properties.

Under the influence of pressure P, the deformation amplitude $\zeta\ (r, \varphi)$ of the diaphragm in the z direction can be

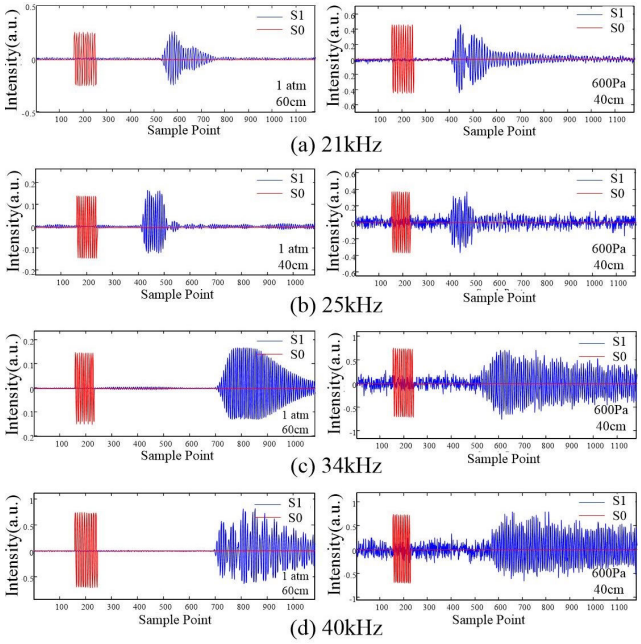

FIGURE 8. (a)-(d): Signals of 21 kHz, 25 kHz, 34 kHz, and 40 kHz under atmospheric environment.

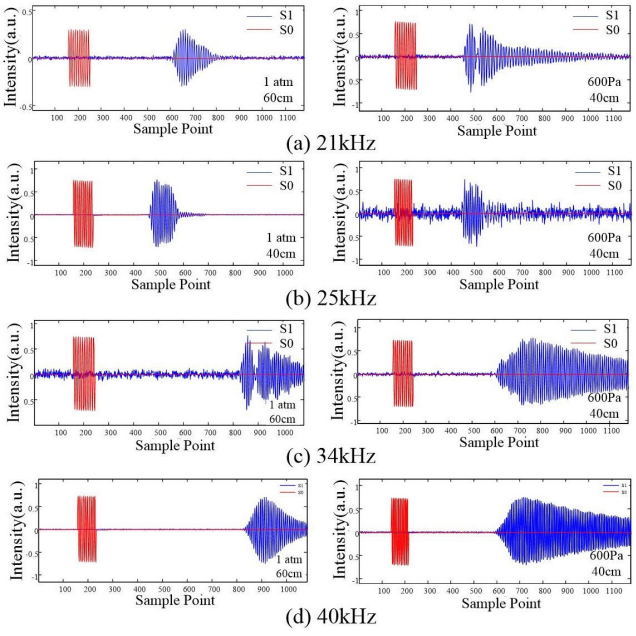

FIGURE 9. (a)-(d): Acoustic signals of 21 kHz, 25 kHz, 34 kHz, and 40 kHz under CO_2 environment.

expressed as:

$$D\nabla^4\zeta = P \tag{3}$$

In Eq.3, $D = Yh^3/12(1-\upsilon^2)$ is the bending rigidity of the diaphragm, and h is the thickness of the diaphragm. For the diaphragm fixed on the cylindrical row structure,

the differential operator is defined as:

$$\nabla^2 = \frac{\partial^2}{\partial r^2} + \frac{1}{r}\frac{\partial}{\partial r} + \frac{1}{r^2}\frac{\partial^2}{\partial \varphi^2} \tag{4}$$

When the pressure acts on the diaphragm, the deformation of the diaphragm is a function of the radial direction r, and the operator is derived by derivation:

$$\nabla^4 = \frac{d^4}{dr^4} + \frac{2}{r}\frac{d^3}{dr^3} - \frac{1}{r^2}\frac{d^2}{dr^2} + \frac{2}{r^3}\frac{d}{dr} \tag{5}$$

Under the boundary condition $r = r_0$, there are $\zeta = 0$ and $d\zeta/dr = 0$, thus:

$$\zeta = \zeta_0(1 - r^2/r_0^2)^2 \tag{6}$$

In Eq. 6, ζ_0 is the deformation of the center position of the diaphragm, and its expression is:

$$\zeta_0 = \frac{3(1-\upsilon^2)r_0^4}{16Yh^3}P \tag{7}$$

For the Fabry-Perot acoustic vibration sensor, the length l of the F-P cavity is determined by the vibration deformation of the diaphragm ζ_0, and the relationship can be expressed as:

$$l = l_0 - \zeta_0 \tag{8}$$

where l_0 is the initial length of the F-P cavity. It can be seen that the length of the F-P cavity is linearly related to the deformation of the diaphragm. Therefore, the relationship between the phase φ of the interference signal reflected by the F-P sensor and the cavity length l of the F-P cavity is as follows:

$$\varphi = \varphi_0 + k\pi l \tag{9}$$

where φ_0 is the initial phase and k is the wave number. Combining Eq.7, Eq.8 and Eq.9, the relationship between the demodulated phase and pressure can be derived as:

$$\begin{aligned}\varphi &= \varphi_0 + k\pi\,(l_0 \pm \zeta) \\ &= \varphi_0 + k\pi l_0 + k\pi\frac{3\left(1-\upsilon^2\right)r_0^4}{16Yh^3}P\end{aligned} \tag{10}$$

It can be inferred from Eq.10 that the phase value will decrease as the pressure decreases, and the experimental results are in good agreement with it as follows.

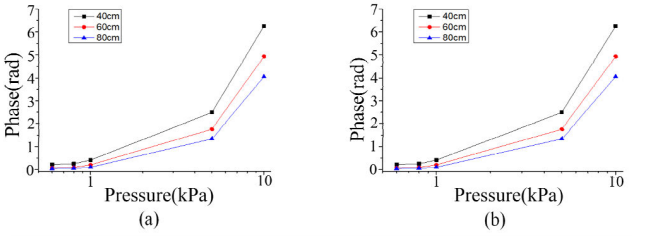

FIGURE 10. (a) Phase-pressure curve of ultrasonic signal of 21 kHz under atmospheric environment. (b) Phase-pressure curve of ultrasonic signal of 21 kHz under CO_2 environment.

As Figure 10 shows, the fiber optic F-P sensor can still receive ultrasonic signals at the distance of 80 cm in both atmospheric and CO_2 environments. At the same distance, the amplitude value of the ultrasonic signal of 21 kHz received by the F-P sensor decreases as the air pressure decreases. At the same air pressure, after the 21 kHz ultrasonic wave propagates 40, 60, or 80 cm, the amplitude value of the ultrasonic signal of 21 kHz received by the F-P sensor decreases with distance. Comparing Figure 10(a) and (b), it can be seen that when the pressure and propagation distance are the same and the amplitude of the signal of 21 kHz in CO_2 gas is generally smaller than the amplitude under atmospheric conditions. However, the speed of the sound wave in CO_2 gas decreases relatively slowly as the pressure decreases. As Figure 10 (b) shows, in the CO_2 environment the signal received by the F-P sensor at a pressure of 10 kPa is greater than the signal received at 100 kPa, and as the pressure continues to decrease from 10 kPa, the received signal shows a decreasing trend.

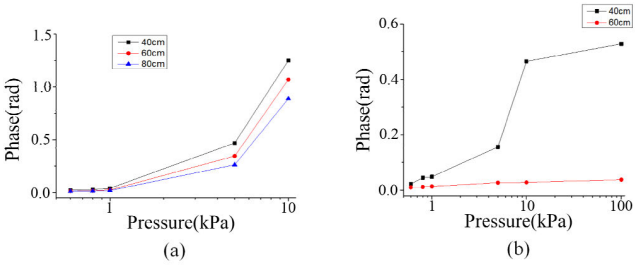

FIGURE 11. (a) Phase-pressure curve of ultrasonic signal of 25 kHz under atmospheric environment. (b) Phase-pressure curve of ultrasonic signal of 25 kHz under CO_2 environment.

As Figure 11 shows, the transmission characteristics of the ultrasonic signal of 25 kHz are similar to those of the 21 kHz signal in both atmospheric and CO_2 gas environments. At the same distance, the amplitude value of the ultrasonic signal of 25 kHz received by the F-P sensor decreases with the decrease of the air pressure. On the other hand, the amplitude value of the ultrasonic signal of 25 kHz received by the sensor decreases as the propagation distance increases. When the pressure and propagation distance are the same, the amplitude value of the received signal in the CO_2 gas is generally smaller than that in the atmosphere. However, in the CO_2 environment, the optical fiber cannot receive ultrasonic signals of 25 kHz at the distance of 80 cm from the F-P sensor. As is shown in Figure 11(b), the amplitude of the ultrasonic signal of 25 kHz detected by the F-P sensor is not significantly reduced when the pressure is reduced from 10^5 Pa to 10 kPa in CO_2 gas environment.

However, the signal detected by the sensor at 80 cm is difficult to distinguish from the noise as the transmission distances of the 34 kHz and 40 kHz acoustic signals are significantly reduced. Therefore, we choose 20 cm, 40 cm, and 60 cm as the test distances. As can be seen from Figure 12 and 13 that the curves in the graphs are similar to the trends under the experimental conditions of 21 kHz and 25 kHz. The signal received by the F-P sensor at the pressure

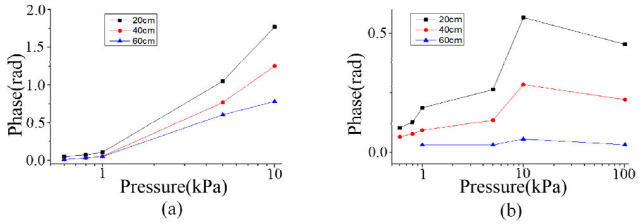

FIGURE 12. (a) Phase-pressure curve of ultrasonic signal of 34 kHz under atmospheric environment. (b) Phase-pressure curve of ultrasonic signal of 34 kHz under CO_2 environment.

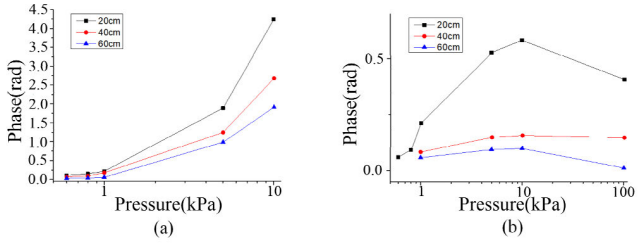

FIGURE 13. (a) Phase-pressure curve of ultrasonic signal of 40 kHz under atmospheric environment. (b) Phase-pressure curve of ultrasonic signal of 40 kHz under CO_2 environment.

of 10 kPa is greater than that at 100 kPa under CO_2 conditions. However the increase here does not affect the downward trend of the entire curve. As the air pressure continues to decrease from 10 kPa, the received signal shows a decreasing trend.

B. ULTRASONIC SOUND VELOCITY ANALYSIS IN ATMOSPHERIC ENVIRONMENT AND CO_2 ENVIRONMENT

The theoretical sound velocity v is related to the parameters of the gas and can be derived from the ideal gas state equation:

$$v = \sqrt{\gamma \frac{RT}{M}} = \sqrt{\gamma \frac{R\,(273.15 + t)}{M}} \tag{11}$$

where γ represents the specific heat ratio of the gas (i.e., the ratio of constant heat capacity to constant heat capacity); R represents the universal gas constant, $R = 8.31\ Jmol^{-1}K^{-1}$; T represents the absolute temperature (K); t represents the temperature in units of °C; and M represents the gas molecular mass. For air, $\gamma = 1.403$ and $M = 28.97\ g\ mol^{-1}$. The internal temperature of the environmental simulation container $t = 15$ °C. Then, according to Eq.11, for an environmental simulation container composed of air, the theoretical sound velocity v of the gas is calculated as:

$$v = \sqrt{1.403 \times \frac{8.31 \times (273.15 + 15)}{0.02897}} \approx 340.54 \tag{12}$$

The inside of the ring-shaped container is filled with air. Under the test conditions of different pressures and different distances, the acoustic signals measured by the optical fiber F-P sensor are shown in Figure 8. By analyzing the waveform of the time-domain of the photoacoustic signal, which is shown in Figure 8, the start time of the waveform of the signal generated by signal generator and the signal received by optical fiber F-P vibration sensor can be determined, as well as the time difference Δt of the two signals. According to Eq.2, the propagation speed of the ultrasonic signals with different pressures and different frequencies in the air environment can be calculated, which is shown in Table 1. The error of sound velocity is calculated by the following equation:

$$\varepsilon = \frac{v_1 - v_0}{v_0} \times 100\% \tag{13}$$

where v_0 represents the theoretical value of the sound velocity and v_1 represents the measured value of the sound velocity.

By analyzing the data in Table 1, when the temperature and humidity are constant, the effects of changes in pressure and frequency on the speed of ultrasonic sound are small and can be neglected. This is consistent with the calculation of the theoretical sound velocity in the gas, which means that the sound velocity is related to the gas composition, humidity, temperature, etc., rather than the pressure and frequency. The theoretical sound velocity in air is 340.54 m/s, and the average value in air from the sound velocity test at room temperature (15 °C) is 336.18 m/s. Compared with the theoretical value, the average error of the sound velocity test value in air is −1.28%. Under the pressure of 600 Pa, the average propagation speed of ultrasonic signals with frequencies of 21, 25, 34, and 40 kHz in air is 336.19 m/s.

For CO_2 gas, $\gamma = 1.304$, $M = 44$ g mol^{-1}, and the internal temperature of environmental simulation container $t = 15$ °C. Thus, according to Eq. 11, for an environmental simulation container composed of CO_2 gas, the theoretical sound velocity of the gas v is calculated as:

$$v = \sqrt{1.304 \times \frac{8.31 \times (273.15 + 15)}{0.044}} \approx 266.39 \tag{14}$$

Filling the inside of the ring-shaped container with air, we measured the acoustic signals with the optical fiber F-P sensor under the test conditions of different pressures and distances, with the results shown in Figure 9.

It can be seen from Table 2 that in the CO_2 gas environment, the effects of changes in the pressure and frequency on the speed of ultrasonic sound are small and can be neglected. The average value of the sound velocity in CO_2 gas at room temperature (15 °C) is tested to be 268.79 m/s. The theoretical result calculated from the formula is similar to 266.39 m/s, and the error of the measured sound velocity is approximately 0.9%. Under the pressure of 600 Pa, the propagation speed of ultrasonic signals of 21, 25, 34, and 40 kHz in CO_2 gas is 271.51 m/s, which is similar to the theoretical result of 266.3 m/s, calculated from the equation. And the error of the measured sound velocity is approximately 0.9%.

C. ANALYSIS OF THE MEASUREMENT ERROR OF SOUND VELOCITY

The main causes of the measurement error of the sound velocity are as follows:

TABLE 1. Acoustic velocity in the air.

Sound speed in air (m/s)	1 atm	10 kPa	5 kPa	1 kPa	800 Pa	600 Pa	Average sound velocity at each frequency (m/s)	Average sound velocity and theoretical sound velocity error of each frequency (%)
21 kHz	335.46	335.69	336.09	336.15	334.32	338.77	336.08	-1.31
25 kHz	335.20	336.09	338.77	334.58	338.77	333.33	336.12	-1.30
4 kHz	336.09	336.98	336.98	335.2	338.77	335.20	336.54	-1.18
40 kHz	338.47	334.58	336.12	334.58	334.58	337.46	335.97	-1.34
Average sound velocity at each air pressure (m/s)	336.31	335.84	336.99	335.13	336.61	336.19	336.18	-1.28
Error from theoretical value (%)	-0.59	0.05	0.49	1.13	2.41	1.92	0.90	--

TABLE 2. Acoustic velocity in CO_2.

Sound speed in air (m/s)	1 atm	10 kPa	5 kPa	1 kPa	800 Pa	600 Pa	Average sound velocity at each frequency (m/s)	Average sound velocity and theoretical sound velocity error of each frequency (%)
21 kHz	268.32	268	268.06	269.74	272.3	271.44	269.64	1.22
25 kHz	263.97	264.03	262.3	275.86	271.19	269.36	267.79	0.52
4 kHz	260.96	270.01	275.32	264.89	276.76	274.29	270.37	1.49
40 kHz	266.01	264.04	265.11	267.09	270.94	270.94	267.36	0.36
Average sound velocity at each air pressure (m/s)	264.82	266.52	267.70	269.40	272.80	271.51	268.79	0.90
Error from theoretical value (%)	-0.59	0.05	0.49	1.13	2.41	1.92	0.90	--

(1) The moving mechanism in the test was used to adjust the distance L between the receiving and transmitting transducers. The calculation of the sound speed was based on the distance value displayed by the control unit of the mechanism. During the test, it was impossible to open the environmental simulation container in order to measure the actual displacement, which causes error in calculating the sound speed. This event is generally the main cause of error in the experiment.

(2) When the receiving transducer moves, the movement causes a slight deformation of the automatic slide rail. There is a level error between the receiving transducer and transmitting transducer; therefore, the actual distance L between the receiving and transmitting transducers is not the horizontal displacement used in the sound velocity calculation, which may cause errors in the calculation.

(3) This study uses the threshold method to determine the initial moment of the excitation signal of the signal generator. The optical fiber F-P sensor receives the initial moment of the signal, and the system calculates the time difference Δt. There is an unpredictable and complex noise in the field environment, which seriously affects the accuracy of the delay estimation and reduces the calculation accuracy of the sound speed.

(4) There is a gap between the flange of the container wall of the ring mold and the cavity of the container, which causes an exchange between the pure CO_2 gas inside the container and the outside atmosphere of the container. The change in the purity of the gas causes the change of the values of γ and M of the gas, affecting the precision of the velocity measurement of sound.

IV. CONCLUSION

Based on the application requirements of ultrasonic sensing technology in the atmosphere of Mars, we established a set of measurement system of low-pressure gas ultrasonic sound velocity to measure acoustic signals under different conditions of gas (air, CO_2) and pressure from 600 Pa to 1 MPa. The optical fiber F-P vibration sensors perform well with high-precision in the ultrasonic sound velocity measurements under different gas compositions, pressures, and center frequencies at 21, 25, 34, and 40 kHz. Theoretical calculations and a large number of experimental results show that the diaphragm-type optical fiber F-P vibration sensor can adapt to low-pressure environments while still receiving ultrasonic signals in 600 Pa CO_2 gas. At the same distance, the amplitude of the ultrasonic signal decreases as the air pressure decreases. At the same pressure, the amplitude of the ultrasonic signal decreases with an increase in the distance. The longest transmission distance of the F-P sensor for which acoustic signals are received is related to the ultrasonic frequency. In the atmospheric environment, when the air pressure is reduced to 1000 Pa, the F-P sensor can receive sound waves of 21 kHz and 25 kHz at the longest distance of 80 cm; meanwhile, sound waves of 34 kHz and 40 kHz can be received at the longest distance of 40 cm. For a reduced air pressure of 600 Pa, the F-P sensor can receive sound waves of 21 kHz at the longest distance of 0.8 m, whereas sound waves of 25 kHz, 34 kHz, and 40 kHz can be received at the longest distance of 0.4 m. In the CO_2 gas environment, with the air pressure reduced to 1000 Pa, the F-P sensor can receive sound waves of 21 kHz, 25 kHz, 34 kHz, and 40 kHz at the longest distance of 0.8 m. For

the air pressure of 600 Pa, the F-P sensor can receive sound waves of 21 kHz at the longest distance of 0.8 m, while sound waves of 25 kHz, 34 kHz, and 40 kHz can be received at the longest distance of 0.6 m. Under identical conditions of frequency, propagation distance, and pressure, the amplitude of the acoustic signal received by the F-P sensor in CO_2 gas is generally lower than that in the air. In the CO_2 environment, the relationship between the sound wave signal received by the F-P sensor and changing pressure is special. For the air pressure near 10^4 Pa, the ultrasonic signal received by the sensor increases significantly, even higher than the intensity at 10^5 Pa. As the air pressure continues to decrease from approximately 10^4 Pa, the ultrasonic signal gradually decreases.

Under the conditions of constant temperature and gas humidity, the propagation speed of the ultrasonic wave is related to the gas composition and unrelated to the pressure and frequency. Under the conditions of room temperature of 15 °C, ambient gas of CO_2, and gas pressure of 600 Pa to 1 MPa, the average velocity of ultrasonic signals at each frequency is 268.79 m/s, which is lower than the 336.18 m/s in air environment. Under the test conditions of room temperature (15 °C), ambient gas of CO_2, and gas pressure of 600 Pa, the propagation speed of ultrasonic signals at each frequency is 271.51 m/s. The sound velocity data in this study measured in the low-pressure CO_2 environment can be applied to theoretical and experimental studies of ultrasonic positioning and detection in future Mars probes.

REFERENCES

[1] K. S. Novak, J. G. Kempenaar, M. J. Redmond, and P. Bhandari, "Preliminary surface thermal design of the Mars 2020 Rover," in *Proc. 45th Int. Conf. Environ. Syst.*, 2015, pp. 1–12.
[2] D. Banfield and R. Dissly, "A martian sonic anemometer," in *Proc. IEEE Aerosp. Conf.*, vols. 1–4, Mar. 2005, pp. 641–647.
[3] E. Chaisson and S. McMillan, *Astronomy Today*. San Francisco, CA, USA: Benjamin Cummings, Jul. 2010.
[4] W. J. Lin, Y. Jia, and C. Li, "Ultrasound propagation in the Martian atmosphere," in *Proc. ICSV*, vol. 24, 2017, pp. 23–27.
[5] J.-P. Williams, "Acoustic environment of the martian surface," *J. Geophys. Res., Planets*, vol. 106, no. E3, pp. 5033–5041, Mar. 2001.
[6] H. E. Bass and J. P. Chambers, "Absorption of sound in the martian atmosphere," *J. Acoust. Soc. Amer.*, vol. 109, no. 6, pp. 3069–3071, Jun. 2001.
[7] A. Petculescu and R. M. Lueptow, "Atmospheric acoustics of Titan, Mars, Venus, and Earth," *Icarus*, vol. 186, no. 2, pp. 413–419, Feb. 2007.
[8] A. Petculescu, "Acoustic properties in the low and middle atmospheres of Mars and Venus," *J. Acoust. Soc. Amer.*, vol. 140, no. 2, pp. 1439–1446, Aug. 2016.
[9] T. G. Leighton and A. Petculescu, "The sound of music and voices in space Part 1: Theory," *Acoustics Today*, vol. 5, no. 3, pp. 17–26, 2009.
[10] T. G. Leighton and A. Petculescu, "The sound of music and voices in space part 2: Modeling and simulation," *Acoust. Today*, vol. 5, no. 3, pp. 27–29, Jul. 2009.
[11] J. Chittenden, V. Chevrier, L. Roe, K. Bryson, R. Pilgrim, and D. Sears, "Experimental study of the effect of wind on the stability of water ice on mars," *Icarus*, vol. 196, no. 2, pp. 477–487, Aug. 2008.
[12] H. E. Bass, L. C. Sutherland, and A. J. Zuckerwar, "Atmospheric absorption of sound—Update," *J. Acoust. Soc. Amer.*, vol. 88, no. 4, pp. 2019–2021, Jun. 1990.
[13] J. Yang, W. J. Lin, and B. Xue, "Experiments of speed of sound in the low pressure atmosphere of Mars," in *Proc. ICSV*, vol. 24, 2017, pp. 23–27.
[14] S. Wu, L. Wang, X. Chen, and B. Zhou, "Flexible optical fiber Fabry–Pérot interferometer based acoustic and mechanical vibration sensor," *J. Lightw. Technol.*, vol. 36, no. 11, pp. 2216–2221, Jun. 1, 2018.
[15] C. Zhou, X. Tong, K. Wang, P. Hu, L. Chen, M. Zhao, and X. Liu, "Research of the differential-type optical fiber F-P vibration sensor with large frequency range," in *Proc. 5th Asia–Pacific Opt. Sensors Conf.*, Jul. 2015, p. 96550.
[16] J. Jiang, T. Zhang, S. Wang, K. Liu, C. Li, Z. Zhao, and T. Liu, "Noncontact ultrasonic detection in low-pressure carbon dioxide medium using high sensitivity fiber-optic Fabry–Pérot sensor system," *J. Lightw. Technol.*, vol. 35, no. 23, pp. 5079–5085, Dec. 1, 2017.
[17] L. Liu, P. Lu, H. Liao, S. Wang, W. Yang, D. Liu, and J. Zhang "Fiber-optic michelson interferometric acoustic sensor based on a PP/PET diaphragm," *IEEE Sensors J.*, vol. 16, no. 9, pp. 3054–3058, May 2016.
[18] F. Guo, T. Fink, M. Han, L. Koester, J. Turner, and J. Huang, "High-sensitivity, high-frequency extrinsic Fabry–Pérot interferometric fiber-tip sensor based on a thin silver diaphragm," *Opt. Lett.*, vol. 37, no. 9, p. 1505, 2012.
[19] B. Liu, J. Lin, J. Wang, C. Ye, and P. Jin, "MEMS-based high-sensitivity Fabry–Pérot acoustic sensor with a 45° angled fiber," *IEEE Photon. Technol. Lett.*, vol. 28, no. 5, pp. 581–584, Mar. 1, 2016.
[20] H. Liao, P. Lu, L. Liu, S. Wang, W. Ni, X. Fu, D. Liu, and J. Zhang, "Phase demodulation of short-cavity Fabry–Pérot interferometric acoustic sensor with two wavelengths," *IEEE Photon. J.*, vol. 9, no. 2, pp. 1–9, Apr. 2017.

JINGCHUAN ZHANG received the Ph.D. degree in instrument science and technology specialty from Tianjin University, China. He is currently a Senior Engineer with the Beijing Institute of Spacecraft Environment Engineering, China. His research interests include measurement and control technology.

YIFEI PEI graduated from the School of Aeronautic Science and Engineering, Beihang University, China. He is currently working as a Senior Engineer with the Beijing Institute of Spacecraft Environment Engineering. His research interests include space environment testing and environment simulation technology.

XIYUAN LI received the master's degree from the School of Aeronautic Science and Engineering, Beihang University, China. He is currently a Senior Engineer with the Beijing Institute of Spacecraft Environment Engineering, China. His research interests include heat and mass transfer.